Chinese Chemical Letters 36 (2025) 109938

Contents lists available at ScienceDirect

Chinese Chemical Letters

journal homepage: www.elsevier.com/locate/cclet

Structure factors dictate the ionic conductivity and chemical stability for cubic garnet-based solid-state electrolyte

Jingyu Shi[a], Xiaofeng Wu[a], Yutong Chen[a], Yi Zhang[a], Xiangyan Hou[a], Ruike Lv[a], Junwei Liu[a], Mengpei Jiang[b], Keke Huang[a,*], Shouhua Feng[a]

[a] State Key Laboratory of Inorganic Synthesis and Preparative Chemistry, Jilin Provincial International Cooperation Key Laboratory of Advanced Inorganic Solid Functional Materials, Jilin University, Changchun 130012, China
[b] Shenyang National Laboratory for Materials Science, Institute of Metal Research, Chinese Academy of Sciences, Shenyang 110016, China

ARTICLE INFO

Article history:
Received 29 January 2024
Revised 18 March 2024
Accepted 28 April 2024
Available online 29 April 2024

Keywords:
Garnet-structured solid-state electrolyte
Structure factors
Ionic conductivity
Chemical stability
Li-ion battery

ABSTRACT

Solid-state electrolytes (SSEs), as the core component within the next generation of key energy storage technologies - solid-state lithium batteries (SSLBs) - are significantly leading the development of future energy storage systems. Among the numerous types of SSEs, inorganic oxide garnet-structured superionic conductors $Li_7La_3Zr_2O_{12}$ (LLZO) crystallized with the cubic $Ia\bar{3}d$ space group have received considerable attention owing to their highly advantageous intrinsic properties encompassing reasonable lithium-ion conductivity, wide electrochemical voltage window, high shear modulus, and excellent chemical stability with electrodes. However, no SSEs possess all the properties necessary for SSLBs, thus both the ionic conductivity at room temperature and stability in ambient air regarding cubic garnet-based electrolytes are still subject to further improvement. Hence, this review comprehensively covers the nine key structural factors affecting the ion conductivity of garnet-based electrolytes comprising Li concentration, Li vacancy concentration, Li carrier concentration and mobility, Li occupancy at available sites, lattice constant, triangle bottleneck size, oxygen vacancy defects, and Li-O bonding interactions. Furthermore, the general illustration of structures and fundamental features being crucial to chemical stability is examined, including Li concentration, Li-site occupation behavior, and Li-O bonding interactions. Insights into the composition-structure-property relations among cubic garnet-based oxide ionic conductors from the perspective of their crystal structures, revealing the potential compatibility conflicts between ionic transportation and chemical stability resulting from Li-O bonding interactions. We believe that this review will lay the foundation for future reasonable structural design of oxide-based or even other types of superionic conductors, thus assisting in promoting the rapid development of alternative green and sustainable technologies.

1. Introduction

Lithium-ion Battery (LIBs) technology has made a significant impact on consumer electronics, electric vehicles, and mass energy storage applications since its development in the late 20th century [1–4]. However, current commercial LIBs exploiting carbon anodes and organic liquid electrolytes are unable to satisfy high energy density and safety demands as modern society develops [5]. Lithium metal has been promoted as a promising anode material for improving battery energy density due to its high specific capacity (~3860 mAh/g) [6]. Nevertheless, uncontrollable Li-dendrite growth and excessive volume expansion during cyclic operations result in poor electrochemical performance and severe safety concerns [7]. In addition, liquid electrolytes composed of multiple salts, solvents, and additives suffer from problems related to easy leakage, facile reaction with electrodes, difficulty in processing, and overheating explosions, resulting in significant limitations on their application in various fields due to the above negative factors. Challenges have been identified with liquid electrolyte LIBs chemistry driving the exploration for high-energy, high-safety, and low-cost manufacturing of advanced SSLBs [8–10].

SSLBs have broken the shackles of conventional LIBs by replacing separators and organic liquid electrolytes with SSEs, enabling lithium metal to serve as anodes, thus boosting energy density in addition to eliminating safety concerns (Fig. 1) [11–13]. Furthermore, SSLBs can also be stacked directly in series to increase the operating voltage as well as maximize space utilization, making them ideally suitable for applications ranging from the

* Corresponding author.
E-mail address: kkhuang@jlu.edu.cn (K. Huang).

https://doi.org/10.1016/j.cclet.2024.109938
1001-8417/

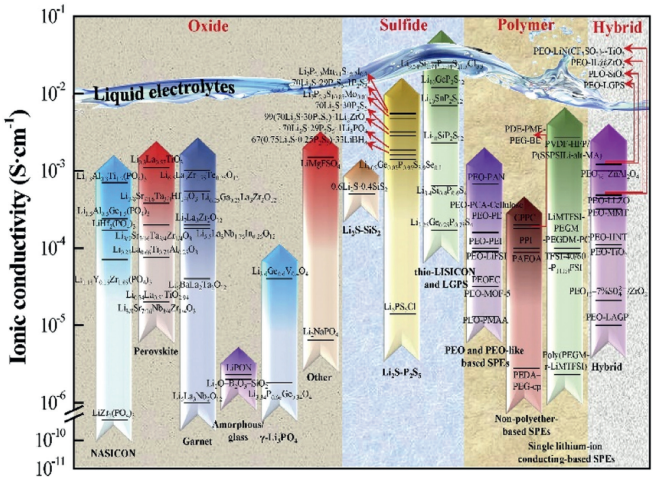

Fig. 1. Comparison of room-temperature ionic conductivity of oxide, sulfide, polymer, and hybrid solid electrolytes. Including NASICON, perovskite, garnet, amorphous/glass, γ-Li_3PO_4, others, Li_2Se-SiS_2, Li_2S-P_2S_5, thio-LISICON and LGPS, PEO and PEO-like-based SPEs, non-polyether-based SPEs, single lithium-ion conducting-based SPEs, and hybrid solid electrolytes. Reproduced with permission [13]. Copyright 2019, Elsevier.

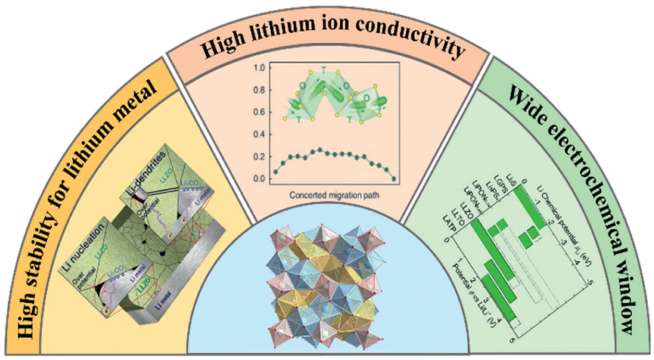

Fig. 2. Cubic LLZO garnet-structured solid-state electrolytes possess a variety of unique properties. (1) Excellent chemical stability to Li metal. Reproduced with permission [38]. Copyright 2020, Wiley. (2) Acceptable ionic conductivity. Reproduced with permission [39]. Copyright 2017, Springer Nature. (3) Wide electrochemical window. Reproduced with permission [37]. Copyright 2015, Royal Society of Chemistry.

medical and military. As an indispensable component within SSLBs, SSEs serve to physically segregate two electrodes preventing direct electron transfer while allowing working ions to transport both charges and masses across the battery, thereby enabling cell reactions to be sustained. Solid polymer electrolytes (SPEs), organic-inorganic hybrid solid composite electrolytes (SCEs), and solid inorganic electrolytes (SIEs) are the three main types of electrolytes found in SSLBs [14]. SPEs are derived from lithium salts dissolved in a solid polymeric matrix, providing the capability for maintaining close contact with rough electrodes even as cell volume changes during cyclic operation due to their low modulus and high flexibility [15,16]. However, polymers with high crystallinity at ambient temperatures severely restrict Li^+ movement resulting in unsatisfactory ionic conductivity ($\approx 10^{-8}$ S/cm), along with inherent limitations associated with poor thermal stability and low mechanical strength, significantly hindering their commercial application [17,18]. SCEs originate from the incorporation of inorganic fillers into ion-conductive engineering organic polymers such as polyethylene oxide, polyacrylonitrile, and polyvinylidene fluoride [19]. The addition of inorganic particles effectively suppresses polymer crystallization, facilitates salt dissociation, as well as enhances its mechanical strength and thermal stability [20]. But SCEs are still plagued with issues related to intrinsic ion conduction and interfaces with electrode materials. Compared to the two polymer-based solid electrolytes mentioned above, SIEs (especially crystalline ionic conductors) are generally composed of frameworks constructed from coordination polyhedrons and mobile species therein [21], offering substantial advantages due to their advances in several of the following aspects: (1) SIEs possess acceptable room-temperature ionic conductivities (10^{-5}–10^{-3} S/cm) and the cationic transference number (theoretically reaches unity) [22,23]; (2) SIEs with high Young's modulus have the potential to prevent lithium-dendrite-induced failures [24,25]; (3) SIEs exhibit excellent thermal stability owing to high decomposition or high-impedance phase transformation temperatures [26]; (4) SIEs are also capable of supporting battery operation at a wide range of temperatures (–50 °C to 200 °C or higher); (5) SIEs are unlikely to experience bulk polarization due to the immobility of their anionic framework, potentially contributing to a higher power density [27].

Interest in SIEs dates back to the observation of ion transport behavior in PbF_2 and Ag_2S by Michael Faraday 200 years ago, followed by the discovery of inorganic solid ionic conductors such as Li_3N, Li-β-alumina, and LIPON that drove further development of this branch [28–30]. Different types of electrolytes possessing distinct microstructures and characteristics present specific advantages, thus classifying SIEs according to their heteroatoms in the ligands into oxides and sulfides [31]. In comparison with sulfide solid electrolytes, oxide solid electrolytes possess an even longer-range development prospect owing to their environmental stability against ambient air, water, and high temperature, as well as offering excellent high energy density and superior safety performance in all-solid-state lithium-ion batteries constructed on them. To date, a wide range of oxide solid electrolytes including LISICON-type, NASICON-type, perovskite-type, antiperovskite type and garnet type have been extensively investigated [7,13,32] However, each SIE differs in its own characteristics from one another, failing to fully satisfy the requirements associated with practical battery application. It is essential to select an oxide superionic conductor with significant advantages that can further be modified, providing an ideal technical route for the development of inorganic SSEs and SSLBs. Among various available SIEs, the cubic phase garnet-type solid electrolyte $Li_7La_3Zr_2O_{12}$ (LLZO) stands out for the following benefits: (1) Acceptable ionic conductivity, capable of reaching a magnitude order of 10^{-3} S/cm at room temperature [33]; (2) Wide electrochemical window, achieved at 9 V in experimental operation [34]; (3) Excellent chemical stability to Li metal, the unique feature of garnets resulting from the absence of reduction as occurs in others [35,36]. Fig. 2 illustrates these advantages more vividly [37–39]. LLZO-based electrolytes are capable of offering an abundance of unique benefits and possibilities for the progress and development of next-generation solid-state batteries.

Inorganic SSEs covering cubic garnet-based oxide ionic conductors and others lie at the heart of the solid-state battery concept. Our aim in this Review is to discuss the current fundamental understanding of the intrinsic properties pertaining to ionic conductivity and chemical stability of garnet-based oxide super-ionic conductors as viewed from the perspective of multifaceted structural properties related to solid-state chemistry. The construction of a more attractive electrolyte structure framework *via* wise manipulation of atoms to construct specific functional elements ultimately lays the foundation for building better next-generation advanced batteries in the near future.

2. Structure-induced modulations in ion transportation with garnet-based SSEs

Li-rich oxide garnets have received widespread scientific attention as fast Li-ion conductors, but their lithium-ion conductivity in

ambient conditions remains 1–2 orders of magnitude lower than that of widely available liquid electrolytes or other superionic conductors such as sulfide-based and halogen-containing solid electrolytes. [28,36,40] Hence, Li-ion conductivity is expected to be further improved *via* microstructural and crystal-chemical engineering. Here we summarize numerous factors that affect cubic garnet Li ion conductivity from a structural perspective, including (1) lithium concentration; (2) lithium vacancy concentration; (3) Li carrier concentration and mobility; (4) Li occupancy at available sites and (5) four readily neglected niche factors. The following sections provide detailed information.

2.1. Structure-dependent evolution of garnet-based oxide ionic conductors

The classic garnet orthosilicate possesses the general chemical formula of $A_3^{II}B_2^{III}(CO_4)_3$ crystallizing in the face-centered cubic structure with the $Ia\bar{3}d$ (230) space group, where A, B, and C are located at the Wyckoff sites in 24c, 16a, and 24d. The oxygen anion occupies the 96h Wyckoff position, constituting 8, 6, and 4 coordination polyhedral with cations A^{2+}, B^{3+}, and M^{4+}. Lithium-containing garnet $A_3^{II}B_2^{III}(LiO_4)_3$ can be readily obtained by substituting lithium for silicon at the C site inside the skeleton [41–43]. Inorganic superionic conductors have achieved a significant advancement with the development of this series of oxides.

Li3: The conventional garnet $Li_3Ln_3Te_2O_{12}$ (Ln = Y, Pr, Nd, Sm-Lu) series compounds were prepared in 2006 with solid-state ceramic methods at temperatures up to 900 °C [44]. Rietveld refinement based on X-ray diffraction (XRD) and Neutron Powder diffraction (NPD) data in combination indicates that these phases adopt the garnet structure (space group $Ia\bar{3}d$). The Ln^{3+} and Te^{6+} cations reside in the dodecahedral and octahedral coordinated sites, as well as Li^+ is accommodated exclusively in the tetrahedral sites commonly occupied in the garnet structure. Edge-sharing of LnO_8 dodecahedron leads to the formation of two interpenetrating body-centered lattices thus building the main framework of $Li_3Ln_3Te_2O_{12}$. The Te^{6+} cations occupy interstitial sites between LnO_8 units, with Te-O distance fluctuating slightly with the size of the elements in the Ln-O framework. The four faces of the LiO_4 tetrahedron in $Li_3Ln_3Te_2O_{12}$ are each shared with a vacant octahedral 48g site. The lattice parameters of the $Li_3Ln_3Te_2O_{12}$ series vary in the range of 12.15970(14) Å (Lu) −12.61596(7) Å (Pr), indicating that the garnet structure is able to accommodate cations of different sizes without changing symmetry. In the case of $Li_3Nd_3Te_2O_{12}$, impedance spectroscopy measurements demonstrated a minimum Li^+ mobility resulting in a maximum conductivity of $\sigma \approx 10^{-5}$ S/cm at 600 °C with an activation energy of 1.22(15) eV. The reason for this can be explained by the fact that lithium remains unchanged in coordination and disorder at temperatures above 300 °C or even 600 °C. However, Li^+ transport in the lattice begins with migration from the tetrahedral site to one of the four neighbouring empty octahedral sites.

The lithium ion in the $Li_3Ln_3Te_2O_{12}$ series is housed exclusively in the tetrahedral 24d site, allowing for a maximum of three lithium ions per formula unit due to its site symmetry [45]. Lithium content can be continuously varied in garnet structures by replacing either Ln^{3+} or Te^{6+} with cations of higher or lower oxidation states to maintain charge balance. Cussen *et al.* replaced Te^{6+} in $Li_3Nd_3Te_2O_{12}$ with Sb^{5+} to drive additional lithium incorporation into the garnet structure to produce $Li_{3+x}Nd_3Te_{2-x}Sb_xO_{12}$ [45]. All compounds crystallize in the space group $Ia\bar{3}d$, with Nd^{3+} at square antiprismatic sites as well as a mixture of Te^{6+}/Sb^{5+} at the octahedral sites conventionally occupied in the lithium-containing garnet structure. It is obvious that lithium cation concentration within the $Li_{3+x}Nd_3Te_{2-x}Sb_xO_{12}$ series is greater than that allowed in conventional garnet stoichiometry. This results in the lithium ions in the structure gradually occupying vacant distorted octahedral 96h sites in addition to residing in the tetrahedral 24d sites. $Li_{3+x}Nd_3Te_{2-x}Sb_xO_{12}$ series compounds exhibit ionic conductivity around 10^{-8} S/cm near room temperature, in sharp contrast to $Li_3Nd_3Te_2O_{12}$ possessing an immeasurably low conductivity below 400 °C. Ionic conductivity increased two orders of magnitude at 400 °C with an increase of 1.7% in lithium content from $Li_3Nd_3Te_2O_{12}$ to $Li_{3.05}Nd_3Te_{1.95}Sb_{0.05}O_{12}$. Activation energy also decreases rapidly from 1.34(2) eV in $Li_3Nd_3Te_2O_{12}$ to 0.672(6) eV in $Li_{3.05}Nd_3Te_{1.95}Sb_{0.05}O_{12}$. The step-change in ionic conductivity and activation energy as a function of composition can be attributed to the incorporation of lithium onto the octahedral site simultaneously with the introduction of vacancies onto the tetrahedral site.

Li5: Cubic $Li_3Ln_3Te_2O_{12}$ undergoes evolution as $Li_5La_3M_2O_{12}$ owing to an increase in lithium ions in the garnet lattice in response to changes in the valence states of the metal ions occupying the A and B positions [46]. NPD experiments indicate that $Li_5La_3M_2O_{12}$ (M = Ta, Nb) series compounds are composed of La^{3+} and M^{5+} in the commonly occurring cubic and octahedral oxide environments similar to the widely recognized $Li_3Ln_3Te_2O_{12}$ garnet structure [47]. The increased lithium content in the $Li_5La_3M_2O_{12}$ garnet tends to raise Li populations at the highly distorted octahedral sites while also introducing vacancies at the tetrahedral sites [40]. Due to the absence of an average structure within the garnet material unit cell length scale, the lithium-containing domains occupying the octahedral sites must necessarily share faces with neighbouring tetrahedral sites, resulting in a portion of the octahedral lithium moving away from the shared surface to reduce the electrostatic repulsion associated with the short Li-Li distance. Li distribution in the two available sites varies with the M ions occupying the 6-fold coordination site [47]. $Li_5La_3Nb_2O_{12}$ and $Li_5La_3Ta_2O_{12}$ both exhibit 0.43 and 0.56 eV electrical conductivity activation energies (<300 °C), as determined from impedance measurements [48]. The high ionic conductivity in these materials may originate from the fact that Li^+ occupies mixed sites enabling the connections between them to form a three-dimensional Li^+ pathway, allowing Li^+ to hop across the pathway with ease.

A series of new member garnet-like structures $Li_{5.5}La_{2.75}K_{0.25}Nb_2O_{12}$ and $Li_{5.5}La_3Nb_{1.75}In_{0.25}O_{12}$ have been yielded based on the partial substitution of trivalent La with monovalent K and of pentavalent Nb with trivalent In in $Li_5La_3Nb_2O_{12}$ *via* the high-temperature solid-state method [49]. XRD revealed that the investigated In- and K-doped compounds are isostructural with the parent $Li_5La_3Nb_2O_{12}$, with the lattice parameters varying as a function of the substituent ion radius. In-substituted $Li_{5.5}La_3Nb_{1.75}In_{0.25}O_{12}$ prepared at 950 °C possesses the highest bulk ionic conductivity of 1.8×10^{-4} S/cm at 50 °C with an activation energy of 0.51 eV among the investigated compounds. Appropriate chemical doping offers a possibility to modify network connectivity *via* controlling the number of readily available vacancies, and therefore facilitating a further improvement of ionic conductivity with garnet-structure related metal oxides.

Li6: Introducing divalent alkaline earth metal ions into the $Li_5La_3M_2O_{12}$ (M = Ta, Nb) garnet-structured ionic conductor is able to further increase Li concentration in the network. Compounds with the chemical formula $Li_6MLa_2Nb_2O_{12}$ (M = Ca, Sr, Ba) were found to crystallize in a cubic phase with the $I2_13$ space group (space group No. 199, $Z = 8$) [50]. A rise in the ionic radius of alkaline earth ions leads to an increase in the cubic lattice parameter. $Li_6MLa_2Nb_2O_{12}$ shares a similar structure to $Li_5La_3M_2O_{12}$ in that rare earth ions occupy the dodecahedral coordination site with transition metal atoms located in the six-fold coordination site. A refinement of the $Li_6MLa_2Nb_2O_{12}$ patterns were achieved by replacing the alkaline earth ions at the lanthanum sites (12b). Excess of lithium in the $Li_6MLa_2Nb_2O_{12}$ garnet structure is dis-

tributed on both the traditional tetrahedral site as well as an additional octahedral site capable of containing six lithium cations per formula unit [51]. Two polyhedrons are connected with the aid of shared faces so that each tetrahedron can be linked to four octahedra, whereas each octahedron has contact with two tetrahedra *via* opposing faces. The Ba-compound $Li_6BaLa_2Nb_2O_{12}$ exhibited the highest ionic conductivity at room temperature (22 °C) with a lower activation energy of 0.44 eV compared to homologous Ca- and Sr-compounds [52,53]. The increased ion mobility for the $Li_6MLa_2Nb_2O_{12}$ (M = Ca, Sr, Ba) series of garnet-based oxides can be attributed to (1) abundant ions capable of hopping from their equilibrium positions and (2) available vacancies with comparable energies in the vicinity with these positions to accept the cations [54–56].

Further adjustments to the amount of divalent alkaline-earth metal ions occupying the rare earth M-site of $Li_5La_3M_2O_{12}$ (M = Ta, Nb, Sn) series of garnet-structured oxides could even increase the concentration of lithium ions per formula unit to 7 [33]! However, despite the fact that the lithium-ion concentration in the garnet structure is close to reaching the upper limit of allowable accommodation, mobile ionic conductivity remains unsatisfactorily stagnant at 10^{-5} S/cm under room temperature. Ion transport ability in ambient conditions is crucial for electrolytes, yet is there any possibility for further enhancement in the conductivity value of garnet structured oxide solid electrolytes?

Li7: Further enrichment of lithium content within garnet-related structure ionic conductors can be realized *via* doping with Zr^{4+} or Sn^{4+} to give compositions of LLZO and $Li_7La_3Sn_2O_{12}$. Awaka *et al.* revealed the exact chemical composition, crystal symmetry, and detailed crystal structure for LLZO based on single crystal X-ray analysis, along with determining the characteristic Li site population in the garnet. LLZO possesses a cubic structure similar to $Li_5La_3M_2O_{12}$, featuring a framework composed of dodecahedral LaO_8 and octahedral ZrO_6 [57]. Lithium atoms occupy the tetrahedral 24d and the distorted octahedral 96h two crystallographic sites at the interstices of the framework structure. The novel crystalline fast lithium-ion conductor LLZO associated with cubic crystallographic system exhibits a total conductivity of 3×10^{-4} S/cm at 25 °C, significantly superior to previously reported garnet-based series solid Li-ion conductors [33]. The tetrahedral LiO_4 and distorted octahedral LiO_6 share the face in the interstice position, facilitating ion migration across the three-dimensional network as a result of the short Li-Li distance. A noteworthy feature of cubic garnet-related Li-ion conductors relates to the excellent Li-ion-conduction properties compared with other materials.

LLZO also crystallized in a tetragonal structure with $I4_1/acd$ (No. 142) space group after sintering at a lower temperature of 980 °C according to Awaka *et al.* in 2009 [58]. The Li-excluded garnet framework was composed of two types of dodecahedral LaO_8 as well as octahedral ZrO_6. Li atoms have been found in three crystallographic sites within the garnet framework structure interstices, including the tetrahedral 8a site Li(1), distorted octahedral 16f site Li(2), and distorted octahedral 32g site Li(3), respectively. Li-vacancy ordering in the tetrahedral sites is able to provide an explanation for the origin of tetragonal symmetry in tetragonal LLZO. The tetragonal LLZO specimen presents a bulk Li-ion conductivity of 1.63×10^{-6} S/cm in addition to a grain-boundary conductivity of 5.59×10^{-7} S/cm at 300 K. About two orders of magnitude lower bulk Li-ion conductivity was observed for tetragonal compared to cubic LLZO at 300 and 320 K. Fig. 3 depicts the evolution of the structure from pristine to stuffed garnet as the concentration of lithium ions per formula unit increases.

A detailed analysis of the findings indicates that a significant difference between cubic and tetragonal LLZO lies in the ordering of lithium atoms and the occupation of lithium sites [57,59]. The Li^+ in cubic LLZO is randomly and partially distributed across three

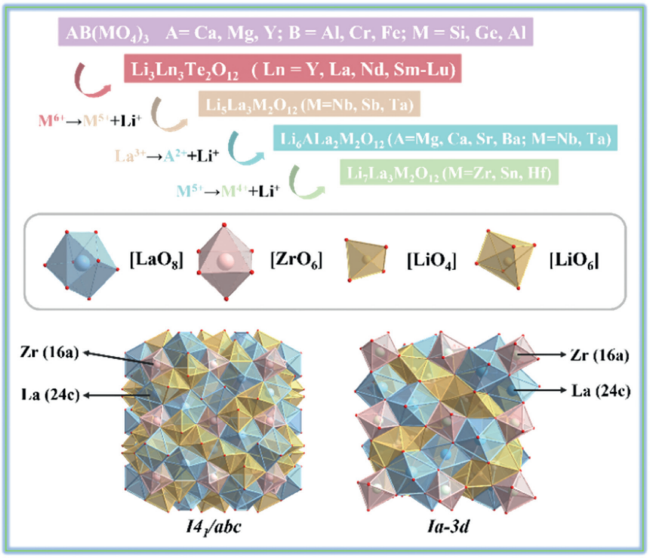

Fig. 3. The structure evolves from pristine to stuffed garnet as lithium ions per formula unit increase.

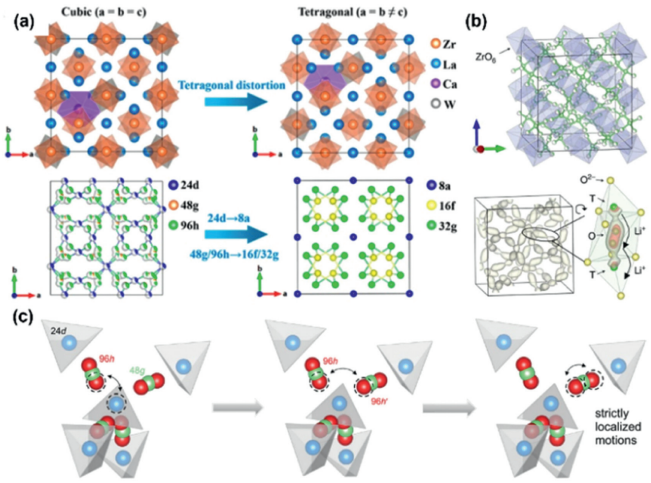

Fig. 4. (a) Crystal structures and arrangement of Li ions for Ca−W dual-substituted c-LLZO and t-LLZO. Reproduced with permission [60]. Copyright 2022, American Chemical Society. (b) The probability density of Li spatial occupancy during AIMD simulations in c-LLZO (the zoom-in subsets show the elongation feature of probability density along the migration channel). Reproduced with permission [39]. Copyright 2017, Springer Nature. (c) Selected Li elementary hopping steps between sites 24d and 96h in LLZMO as evidenced by NPD. Reproduced with permission [61]. Copyright 2015, American Chemical Society.

sites, consisting of the tetrahedral 24d site, six-fold coordinated 48g site, and its distorted four-fold-coordinated split 96h site. The transition from the cubic to tetragonal phase results in a tetragonal distortion, converting the 24d sites of the cubic phase into fully occupied 8a sites, as well as the partially occupied 48g/96h sites of the cubic phase are transformed into two completely filled 16f and 32g sites (Fig. 4) [60,61]. Tetragonal distortion produces a significant shift in the lithium-ion distribution and decreases the ionic conductivity.

2.2. Structural factors affect the conductivity of Li7 series solid-state electrolytes

2.2.1. Li vacancy concentration

As described above, LLZO adopts both tetragonal ($I4_1/acd$) and cubic phase ($Ia\bar{3}d$) two distinct crystallographic structures. Pure

LLZO prefers to crystallize into the more thermodynamically stable tetragonal phase with an ordered Li distribution at room temperature rather than the cubic phase, whereas its ionic conductivity (10^{-6}–10^{-5} S/cm) is roughly 1–2 orders of magnitude lower than that of cubic [62]. Therefore, stabilizing the cubic phase is imperative in order to obtain highly conductive LLZO. Super valent elemental doping has proven to be effective in stabilizing the cubic phase by introducing lithium-ion vacancies in the structure interstices and increasing the disorder of the Li sublattice [38,63,64]. To date, substitutions that have been performed include Al, Fe and Ga for Li; Ca, Sr, Ce and Y for La; Nb, Ta, W and Mo for Zr [43,65-68]. Guo *et al*. investigated the effects of Ga on the garnet phase transition, revealing that garnet-type materials exhibited cubic structures at Ga concentrations exceeding 0.20 Ga per formula unit, but lower Ga concentrations resulted in the coexistence of cubic and tetragonal phases [65]. A minimum of 0.40 mol of Li vacancies is required according to the results to stabilize the cubic phase. Similar cubic phase stabilization is also observed with Bi substitution, along with critical lithium vacancies at the same concentration as Bi appearing in the framework. The subcritical doping composition $Li_{6.8}La_3Zr_{1.8}Bi_{0.2}O_{12}$ associated with the cubic crystal system demonstrates that per formula unit requires 0.2 mol Li vacancies in order to stabilize the cubic polymorph of Li-stuffed garnet [69]. It was recently shown by Yu *et al*. that a stabilization of the cubic garnet $Ia\bar{3}d$ modification could also be achieved with the partial dual-substitution of Ca^{2+} at the La^{3+} and W^{6+} at the Zr^{4+} sites [60]. The present study suggests that a critical Li vacancy concentration (0.5 mol per formula unit) is necessary for cubic LLZO to be stabilized [70–73]. The exact amount of Li vacancies necessary to stabilize cubic LLZO owing to differences in substitution sites remains ambiguous but with estimates ranging from 0.125 mol to 0.5 mol [43].

As a quantum mechanical calculation method, density functional theory (DFT) can provide detailed information about the microscopic physical properties of materials such as their electronic structure, band structure, and charge density distribution, essential for understanding and predicting the mechanisms of ion transport in solid electrolytes. DFT was also employed to assist in predicting the concentration of precise lithium vacancies per formula unit required to stabilize the cubic crystal system LLZO. Santosh conducted DFT calculations to demonstrate that high Li^+ vacancy concentrations can increase lithium-ion conductivity since they provide mobile ion individuals [74]. It is consistent with the LLZO with a higher lithium vacancy concentration (0.4–0.5 mol) exhibiting the maximum ionic conductivity at room temperature as proposed by Thangadurai [43]. The predicted critical Li vacancy concentration needed to obtain cubic LLZO determined by the computation agrees with the experimental results where substitution is performed on the Li sublattice, but demonstrates a divergence upon super valent substitution is carried out on Zr. The possible reason for this is that during the thermal treatment of the super valent cation-substituted specimens with the alumina crucible, partial Al accidentally enters the lithium lattice in addition to the intentionally doped cations, resulting in a higher concentration of Li vacancies than expected [75–77].

The presence of Li vacancies in garnet-structured oxide superionic conductors can not only serve to stabilize their cubic phase but also lead to improved ion transport properties [43]. It is generally acknowledged that the ionic transport in crystalline solid ionic conductors is dominated by the vacancy mechanism, depending on Schottky defects that create numerous vacancies available for ion hopping among the crystals [20]. Ion transportation is able to be achieved *via* hopping the mobile ions between vacancies, thus requiring more vacancies on the equivalent (or nearly equivalent) sites in comparison to the number of mobile ions in the framework structure. Mo *et al.* elaborated in detail based on *ab initio* models explaining why garnet-structured superionic conductors rich in lithium-available vacancies are able to deliver exceptionally high ionic conductivity compared to typical solids [39]. Due to the fact that the Li ions in LLZO partially co-occupy the tetrahedral and octahedral sites, both the tetrahedral-site Li ions hop to the nearest-neighbor octahedral sites and the Li ions occupying these octahedral sites into their nearest neighbor tetrahedral sites, thus enabling multiple Li ions migrate concerted along the 3D diffusion channel (Fig. 4b). The solid-state nuclear magnetic resonance (NMR) technique is capable of detecting local structure information at different time/length scales for an intuitive understanding of the ion dynamics in highly conductive garnet-structured ion conductors from an experimental perspective [61,78-80]. Yang *et al*. applied high-resolution solid-state NMR to monitor the impact of Li vacancies created by W substitution at Zr sites within garnet skeleton on ionic conductivity properties, a behavior that promotes the rearrangement of Li ions across the available tetrahedral as well as the octahedral crystallographic positions at the interstitial structure for optimal transport along the 24d-96h-48g-96h-24d route [79]. Solid state magic-angle spinning nuclear magnetic resonance (MAS NMR) provides evidence that at a substitution level of $x = 0.150$, $La_3Zr_2Li_{7-3x}Ga_{x\square 2x}O_{12}$ is capable of achieving a stable cubic phase with an optimum proportion of charge carriers and vacancies in the face sharing tetrahedral-octahedral channels, thus facilitating lithium transport [80]. The total conductivities measured *via* electrochemical impedance spectroscopy were as high as 1.3 and 2.2 mS/cm at 24 and 42 °C, respectively. LLZO with lithium vacancy concentrations in the range of 0.4–0.5 mol has been known to reach a maximum in ionic conductivity under ambient conditions [62]. Nevertheless, excess Li vacancies are likely to reduce ionic conductivity owing to the ion trapping effect causing a decrease in mobile Li^+ concentration.

2.2.2. Li carrier concentration and mobility

Under the premise of effectively stabilizing the cubic phase in LLZO based on strategies such as introducing lithium vacancies, further fine-tuning the lithium ion concentration in the garnet structure *via* the charge difference between hosting cations and substituents is able to achieve the optimum conductivity [21,81]. LLZO-based components are observed to exhibit excellent ionic conductive properties at lithium content in the range of 6.1 to 6.8 (below the theoretical limit of 7.5) as summarized in the published studies [43,82]. It is noteworthy that the conductivity in the garnet-structured ionic conductor does not increase linearly with the lithium-ion concentration, either from structural evolution in the Li3-Li7 series or to framework modifications in the Li7 series. This is due to the fact that the garnet family of materials is not subject to the ionic Hall Effect, resulting in only a limited number of lithium ions in the structural interstices participating in the conduction process. In terms of the Nernst-Einstein-Smoluchowki equation: $\sigma = \mu q \eta$, where μ is the carrier mobility, q is the electronic charge, and η is the mobile charge carrier concentration. Ionic conductivity for garnet-based ion conductors is governed by the combination of effective concentration and mobility for Li since the charge is fixed at 1 [83].

Nozaki *et al.* investigated the diffusion behavior of lithium ions in garnet-type oxides $Li_{5+x}La_3Zr_xNb_{2-x}O_{12}$ ($x = 0$–2) with the assistance of both positive muon-spin relaxation and *quasi*-elastic neutron scattering techniques [84]. The results reveal that the diffusion coefficient for Li^+ does not vary with dopant, thus the amount of mobile Li^+ in the garnet lattice is the predominant parameter for determining σ_{Li}, involving only 10%−15% of Li-ion serving as carriers. Subsequently M. Ahmad estimated the actual concentration of mobile Li^+ in garnet LLZO based on the conductivity spectra at different temperatures, obtaining an average value of 3.17×10^{21} cm^{-3} as an indication that only 12.3% of the total Li^+ contains is capable

of contributing to conduction [85]. This ratio is in accordance with previous findings without variation with respect to temperature. In addition, LLZO possesses a diffusion coefficient of 1.33×10^{-8} cm^2/s at room temperature, comparable to that of other fast Li^+ conductors. Ga was systematically introduced into the Li tetrahedral 24d site in LLZO by Guo *et al*., thus providing evidence that the concentration of mobile lithium ions is on the order of 10^{21} cm^{-3}, mobility is on the order of 10^{-7}–10^{-6} $cm^2\,V^{-1}\,s^{-1}$, and the jumping rate is on the order of 10^7 rad/s at Ga concentration of 0.2–0.4 mol per unit molecular formula for −10 °C [65]. The concentration of mobile lithium ions in the $Li_{7-3x}Ga_xLa_3Zr_2O_{12}$ specimens is similar to the previous pristine LLZO, but the mobility, diffusion coefficient, and jumping rate have been significantly improved. Another noteworthy finding is that the carrier concentration, mobility and diffusion coefficient in the $Li_{7-3x}Ga_xLa_3Zr_2O_{12}$ system exhibit unpredictable variations with changes in dopant concentration and temperature, differing dramatically from the results of previous experiments. The recently reported Al-doped $Li_7La_{3-x}Al_xZr_2O_{12}$ (x = 0, 0.1, and 0.2) garnet-type electrolytes demonstrate temperature-dependent Li^+ ion concentrations, ion mobility, hopping rates, and diffusion coefficients, with the samples all exhibiting increasing behavior as the temperature rises [86]. The relationship between ionic conductivity, carrier concentration, and mobility in garnet-structured solid electrolytes remains to be thoroughly investigated, hindering the development of high-performance solid electrolytes for energy storage and conversion. Therefore, a deeper understanding of correlated factors is necessary to fully exploit the potential for garnet-based solid electrolytes.

2.2.3. Li occupancies at available sites

As reported in the literature, lithium-ion occupancy at available tetrahedral and octahedral sites has a significant impact on the overall lithium mobility in garnet-structured electrolytes [87]. Lithium occupies all 24d tetrahedral sites while vacating the octahedral sites empty in the pristine garnet phase $Li_3Nd_3Te_2O_{12}$, resulting in an unmeasurable conductivity at room temperature since lithium is believed to be immobile in this arrangement. A rising lithium content in per formula unit leads to lithium redistribution with decreases in tetrahedral occupation and increases in octahedral, thereby affecting lithium mobility [42]. There is a decreasing trend in 24d site occupancies of 80%, 67%, and 56% for $Li_5La_3Ta_2O_{12}$, $Li_6BaLa_2Ta_2O_{12}$, and LLZO, but a steady increase in octahedral site occupancies of 43%, 64%, and 90% have been observed, corresponding to the rise in ionic conductivity values under ambient temperature from 10^{-6} to 4×10^{-5}, and eventually reach 3×10^{-4} S/cm [85]. The evolution of the structure-conductivity relationship from Li3 to Li7 series highlights this correlation.

The relationship between lithium ionic conductivity, mobility, and carrier concentration has been explored in the garnet series over the composition range $Li_{7-x}La_3Zr_{2-x}Ta_xO_{12}$ (x = 0.5, 0.75, and 1.5) based on neutron and synchrotron diffraction [83]. Increasing the lithium population at the 96h site and depopulating the 24d site as lithium concentration rises leads to a nonlinear increase in ionic conductivity, demonstrating that the effective carrier concentration is dependent on lithium site occupancy. Llordés *et al*. proposed a dual substitution strategy $Li_{6.55+y}Ga_{0.15}La_3Zr_{2-y}Sc_yO_{12}$ for studying the ion conductivity of cubic garnets with $n_{Li} > 6.55$, in which Ga substitution was aimed at stabilizing the cubic crystal structure as well as Sc was incorporated to increase the number of charge carriers [75]. The presence of Sc contributes to the disorder of the lithium network at the local scale allowing for a broader distribution of chemical environments, leading to an increase in the regional mobility of the Li population. Further Sc substitution results in Ga occupying octahedral 96h sites, thus suppressing the ionic diffusion owing to possible obstruction of the lithium percolation network. Lithium occupying the 96h site exhibits high local mobility facilitating long-range ion diffusion, coincident with garnet $Li_{6.65}Ga_{0.15}La_3Zr_{1.90}Sc_{0.10}O_{12}$ possessing 1.8×10^{-3} S/cm high ionic conductivity at 300 K. Yu *et al*. adopted the similar approach for incorporating Ca^{2+} into the La^{3+} site together with W^{6+} into the Zr^{4+} site, that not only effectively stabilizes the garnet in cubic phase but also reduces the endothermic enthalpy during the synthesis [60]. Synchrotron X-ray powder diffraction (SXRD), NPD, and MAS NMR in combination revealed that Ca−W dual substitution has regulated the local lithium framework *via* raising Li^+ occupancy at the 96h site, leading to a significantly lower Li^+ migration barrier and thus increasing the ionic conductivity from 2.98×10^{-6} S/cm to 5.74×10^{-4} S/cm in two orders of magnitude. Recently, Ferguson *et al*. analyzed the association between lithium site occupancy and ion conductivity in high lithium concentrations in the range of 6.70–7.15 mol per formula unit [88]. Tantalum-doped $Li_{6.75}La_3Zr_{1.75}Ta_{0.25}O_{12}$ system exhibits an increase in lithium occupying the 96h octahedral sites with rising lithium content, while Li occupying the 24d tetrahedral sites decreased. Increasing lithium-ion conductivity to $3\text{-}5 \times 10^{-4}$ S/cm at various lithium stoichiometries is closely associated with the octahedral Li site occupation from 0.78 to 0.87. In addition, Goodenough and his co-workers even suggested that the Li^+ occupancy/vacancy ratio of 3:1 for octahedral sites is the optimum for achieving high ionic conductivity [70]. The enumeration of findings provides the foundation for future designing superionic conductors with garnet backbone structures by modulating the concentration of lithium ions per formula unit in order to optimize the distribution among the available sites, thereby maximizing the effective carrier concentration and boosting ionic conductivity.

2.2.4. Other structural-related influencing factors

In addition to the various factors discussed above, the lattice constant for garnet-structured oxide ceramic electrolytes also possesses a close relationship with the ion transport characteristics [18,36]. The reason for this is that elemental substitution-induced lattice expansion may lead to an increase in the polyhedral volume of LiO_4 and $(M/La)O_8$ in the garnet framework thus expanding Li-ion interstices for hopping, ultimately bringing about high ionic conductivity. There is evidence to suggest that the highest lithium-ion conductivity within garnet-type frameworks can be achieved at lattice parameters in the range of 12.91–12.98 Å irrespective of the position of substitution and the corresponding substitution elements with constant or varying lithium content [43]. Recently, Kireeva *et al*. presented further evidence for the existence of optimal lattice parameters and confined the value within the interval 12.950–12.965 Å, corresponding to the optimum Li ionic conductivity σ_{tot} as well as the lowest activation energy E_a [89]. Al, Ga, and Fe incorporation into lithium lattice provides an additional contribution to the modification of this range whereas the specific impact of these dopants is of complex character.

Lithium ions diffusing in the garnet structural interstice are required to cross the face of a regular triangle shared by tetrahedral vacancies and octahedral vacancies where the circumferential radius of the triangle is defined as the bottleneck size, which is the minimal migratory channel for lithium that has a significant impact on Li-ion conductivity [90]. Huang *et al*. obtained the medium-entropy ceramic oxide superionic conductor $Li_6La_3Zr_{0.5}Hf_{0.5}Ta_{0.5}Nb_{0.5}O_{12}$ *via* incorporating four metal elements in equimolar ratios at the Zr 16a position of the garnet skeleton. The neutron pair distribution function (PDF) reveals that the four introduced ions do not occupy 16a at random, instead exhibiting local clustering where pentavalent ionic octahedrons are preferred to be surrounded by tetravalent ionic octahedrons [90]. This behavior contributes to the enlargement of the bottleneck size from the pristine Ta-LLZO circle radius of 1.8100 Å with a triangle area of 4.2366 $Å^2$ to the ME-LLZO circle radius of 1.8463 Å with a triangle

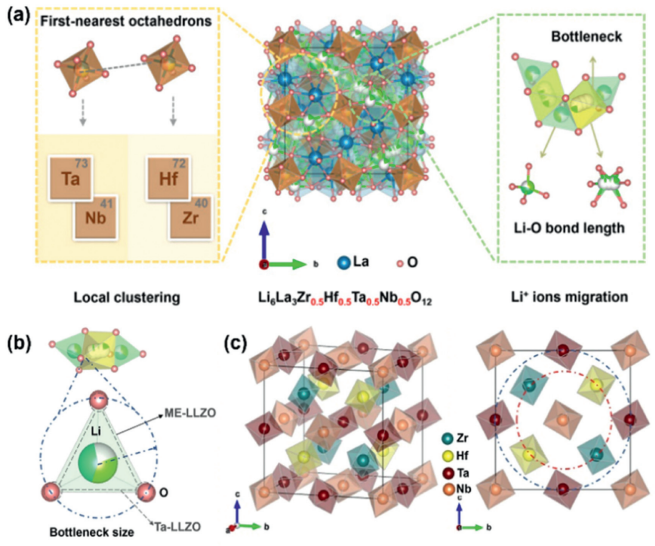

Fig. 5. (a) Schematic diagram of the medium-entropy garnet $Li_6La_3Zr_{0.5}Hf_{0.5}Ta_{0.5}Nb_{0.5}O_{12}$ structure. (b) The bottleneck size of ME-LLZO (solid lines) and Ta-LLZO (dotted lines). (c) The occupancy of Zr^{4+}, Hf^{4+}, Ta^{5+}, and Nb^{5+} at the 16a site in the lowest energy supercell. Reproduced with permission [91]. Copyright 2023, Elsevier.

area of 4.3946 $Å^2$. The enlarged bottleneck size combined with the weakened Coulomb force between Li-O endows ME- LLZO with an ion conductivity of 3.3×10^{-4} S/cm at room temperature and an activation energy of 0.44 eV (Fig. 5) [91]. Molecular dynamic simulations have also been carried out to investigate the effect of bottleneck size between the polyhedron of 24d and 96h sites in cubic LLZO on lithium ion diffusion [92]. In addition to the unneglectable discreteness between the lattice constant and lithium-ion diffusivity, there exists a *quasi*-linear relationship between bottleneck size and lithium-ion diffusivity at 1000–1400 K high temperatures. Two peaks associated with the contact surfaces between tetrahedra and octahedra in the lithium-ion migration pathway can be visualized in the energy barrier diagram for face-centered cubic LLZO crystals, as well as further adjustment of the bottleneck dimensions with appropriate equivalent elemental doping can lead to a greater reduction of the activation energy of the lithium garnet by 40%.

The preparation of LLZO single crystals or polycrystalline pellets under a high-temperature environment is known to result in lithium being highly volatile. Missing lithium ions in LLZO can be regarded as negatively charged acceptor defects from the perspective of inorganic solid-state chemistry, in which case the presence of oxygen vacancies is able to act as positively charged donors in order to balance lithium vacancy defects [64,93]. *Via* isotope exchange depth profiling with $^{18}O_2$ as a stable isotope tracer followed by time of flight secondary ion mass spectrometry (ToF-SIMS) analysis, Kubicek *et al.* verified the presence or even abundance of oxygen vacancies in all investigated garnet materials including single crystals, polycrystals, and various cation substituents (Ta^{5+}, Ga^{3+}, and different Al^{3+} concentrations) [94]. The oxide tracer diffusion coefficient at 350 °C is surprisingly high (up to $D^* = 8.2 \times 10^{-12}$ cm/s) even comparable to that of Yttria-stabilized zirconia, a fast oxygen-ion conductor. However, the impact of oxygen vacancies on lithium ion transport in LLZO has yet to be clarified, and the reason behind this is that (1) oxygen vacancies serving as donors lead to reduced Li stoichiometry; (2) oxygen vacancies can affect phase formation and stabilization *via* elastically deforming the LLZO lattice; (3) elastic deformations are able to further influence Li^+ migration barriers and conduction paths in LLZO depending on the exact location of oxygen vacancies in the lattice [95]. A case-by-case analysis is required to determine the precise impact of the defect chemistry regulation. Yu *et al.* have recently fabricated Ta-doped LLZO garnet solid electrolytes by modulating sintering atmospheres in order to investigate the implications of oxygen vacancies on the physicochemical properties of such oxide ionic conductors [95]. The occurrence of oxygen vacancies was found to have a detrimental impact on the garnet ceramic specimen phase purity, mechanical strength, ion transport properties, and even symmetric as well as solid-state batteries assembled based on them. A more comprehensive understanding of oxygen vacancies with garnet-type solid electrolytes is expected to be required in the future to improve the electrochemical performance of oxide superionic conductors and even SSLBs through rationally controlling and utilizing oxygen vacancies.

Ion mobility in garnet electrolytes can also be influenced by the bonding length between the mobile ions and their surrounding ions in the local structure. On the one hand, the diffusion of Li ions in the three-dimensional channel within the cubic garnet structure is required to cross the triangular O^{2-} neck between LiO_4 tetrahedra and LiO_6 octahedra, implying that the length of Li-O bonds has a significant direct impact on Li ions migration [91]. On the other hand, the Li-O bond length is able to reflect the strength of the bond between ions, affecting the activation energy required for Li to jump from one site to another, a property that is crucial to its application in the solid-state battery [96,97]. It will be necessary to gain a deeper understanding of the behavior of Li-O bonds in different environments in order to optimize lithium-based energy storage systems in the future.

Li concentration, Li vacancy concentration, Li carrier concentration and mobility, Li occupancy at available sites, lattice constant, triangle bottleneck size, oxygen vacancy defects, and Li-O bond interactions in cubic lithium-rich garnet sublattices are capable of being manipulated in order to regulate the distribution of lithium ions at available sites in interstitial tetrahedra and octahedra, optimize the three-dimensional anisotropic ion transport path, and decrease the energy barriers for the Li^+ ions to pass through during migration, so as to realize the fast and synergistic ion migration.

In addition to the structural modulation induced by element doping mentioned above, controlling sintering temperature as well as introducing secondary phases are also effective in achieving LLZO ($Li_7La_3Zr_2O_{12}$). In general, regulating the sintering temperature in the range of 1100 °C to 1200 °C is more favorable for cubic phase generation. This is due to the fact that in this temperature range, grains can grow moderately without experiencing excessive grain growth and phase transformation caused by high temperatures. However, it should be noted that the optimal sintering temperature range is also affected by the material composition and the sintering environment [98]. Additionally to modulating the sintering temperature, introducing secondary phases (such as Li_2O, $La_2Zr_2O_7$) into LLZO can also facilitate the formation of cubic phases. The reason behind this is that certain doping elements are able to lower the energy barrier for cubic phase formation, allowing them to exist at lower temperatures or over a broader range of compositions [7]. In summary, the application of these strategies not only achieves the phase stability of LLZO and optimizes the structure and performance of the material, but also provides a reliable methodology for the development of high-performance solid-state electrolytes, laying the groundwork foundation for the advancement of future solid-state battery technology.

3. Relationship between cubic garnet-based solid electrolyte structure and chemical stability

The SSEs serve as the key component to realize solid-state batteries, hence not only be required to meet the key criteria of high Li-ion conductivity but also excellent chemical stability [6]. Poor

chemical stability of a material may induce undesirable reactions in the ambient air further resulting in poor battery performance or safety concerns. Therefore, designing and manufacturing highly chemically stable electrolytes with the ability to maintain their initial structure and composition intact even after prolonged exposure to moisture is of great significance for the practical application of all-solid-state batteries [99]. This motivates us to summarize several structural elements that have an impact on the chemical stability of garnet-based SSEs from the crystallographic perspective with the intent of gaining a thorough understanding of their reaction mechanisms in order to assist in the future rational design of oxide-based superionic conductors.

3.1. Structural impacts on garnet-based ion conductor chemical stability

Garnet-structured series solid electrolyte was widely accepted as air-resistant during its early stages of discovery. However, Cheng *et al*. combined surface-sensitive characterization techniques revealed that LLZO had experienced corrosion and produced a Li_2CO_3 layer with a thickness of nearly 10 nm after air exposure only for a few days [100]. The chemical instability of garnet-based solid electrolytes gradually came to light afterward. Research has revealed that contamination on garnet-type ceramic surfaces interferes with ionic transport, resulting in poor interfacial wettability and high resistance, leading to lithium dendrite growth and rapid capacity degradation [101]. Considering this, this subsection begins with a discussion on the evolution of the chemical stability of a garnet-structured series of SSEs as a function of lithium-ion concentration. We subsequently dissect the effects of multiple structural parameters within the framework on air stability with respect to a classical garnet oxide superionic conductor LLZO, with a view to developing enhanced air-stable materials in the near future.

3.1.1. Li^+ concentration

The concentration of lithium ions per formula unit in solid electrolytes with garnet structure not only affects the anisotropic transport of mobile ions in the framework but also plays a significant role in determining their chemical stability.

Li3: Galven *et al*. evaluate the chemical stability of the Li3 series garnets solid ionic conductor *by* placing the platinum crucible containing 0.5 g of $Li_3Gd_3Te_2O_{12}$ and $Li_3Nd_3Te_2O_{12}$ specimens in a reactor containing 20 drops of water while applying a CO_2 pressure of 10 bar and heating the reactor (125 cm^3) at 140 °C for one night [102]. There was no trace of Li_2CO_3 in the PXRD pattern resulting from the reaction, and no variation in cell parameters before and after the process indicating that no Li^+/H^+ exchange had taken place. The Li^+/H^+ exchange reaction between garnets and H_2O is predominantly responsible for the instability of garnets against moisture. Research-based experimental results demonstrate that Li3 series testing garnets exhibited superior chemical stability without suffering erosion or contamination in an environment containing water and carbon dioxide.

Li5: Franck *et al*. revealed the feasibility of Li^+/H^+ exchange in $Li_5La_3Nb_2O_{12}$ garnet ionic conductors within the Li5 series based on regular qualitative and quantitative characterization [103]. $Li_5La_3Nb_2O_{12}$ garnet exhibits incomplete ion exchange with acetic acid solution in contradiction with a result published by Truong and Thangadurai, but multiple measurements indicate that the exchange rate is capable of reaching 72.3% hence further confirming its chemical instability [104]. Divalent alkaline-earth-metal ions (Ca, Sr, Ba) are able to be introduced into the La dodecahedral sites in the $Li_5La_3Nb_2O_{12}$ garnet skeleton further increasing the lithium content per formula unit. High lithium content $Li_{5+x}Ba_xLa_{3-x}Nb_2O_{12}$ (x = 0, 0.5, 1) series compounds are still prone to H^+/Li^+ exchange reactions in water at room temperature similar to the Li5 series homologs, suggesting the chemical instability of conducting materials in this class. However, the ion exchange proceeds to a lesser extent with an increase in barium and lithium content. It is noteworthy that Thangadurai *et al*. have experimentally demonstrated that the ion-exchange reaction in garnet-type $Li_{5+x}Ba_xLa_{3-x}Nb_2O_{12}$ is reversible and even able to reproduce the original conductivity [104]. Taking into account that the specificity of substitution sites may have an impact on the chemical stability of garnet structural ionic conductors, the incorporation of Y into the $Li_5La_3Ta_2O_{12}$ garnet Ta octahedral site presented in Thangadurai *et al*. will provide an answer to this question [105]. $Li_{5+2x}La_3Ta_{2-x}Y_xO_{12}$ (x = 0.50 and 0.75) was treated with the 1 mol/L LiCl aqueous solution with the pH reached a maximum of 11–11.5 from an initial value of 6 and remained almost constant for the rest of the week. The variation in pH is able to demonstrate the exchange of Li^+ with protons in $Li_{5+2x}La_3Ta_{2-x}Y_xO_{12}$. The above results indicate that the Li5 series garnet consistently exhibits chemical instability regardless of elemental substitution or substitution sites.

Li6: Galven *et al*. revealed that $Li_6BaLa_2Nb_2O_{12}$ Li-stuffed garnet belonging to the Li6 series was also capable of undergoing spontaneous Li^+/H^+ exchange in ambient air but with slower kinetics [106]. Elevating the temperature is able to contribute to speeding up this reaction process. Furthermore, $Li_6BaLa_2Nb_2O_{12}$ is unstable at high temperatures from 600 °C to 750 °C in the presence of CO_2, as well as CO_2 absorption/desorption process associated with Ba expulsion/reintroduction is not completely reversible. This work has further provided evidence that the Nb-based garnet analogy $Li_6BaLa_2Ta_2O_{12}$ is as well unstable in humid air at low temperatures, exhibiting spontaneous ionic exchange and Li_2CO_3 formation with released lithium. Thangadurai *et al*. inferred from the data obtained *via* thermogravimetric analysis that $Li_6BaLa_2Nb_2O_{12}$ garnet at room temperature exhibits an ion exchange degree of 20% with respect to water [104]. This implies that ion exchange does not cease to take place in $Li_6BaLa_2Nb_2O_{12}$ garnet in spite of low exchange rates. The behaviors of the aforementioned two typical oxide ionic conductors are similar to that of Li5 series garnets where the lithium quantity is greater than that can be accommodated at the structural interstitial tetrahedral sites.

Li7: As already mentioned, the representative material LLZO belonging to the Li7 series is found to exist in two distinctive geometrically symmetric crystal systems, tetragonal and cubic, depending on the lithium position in the architecture constructed from LaO_8 dodecahedron and ZrO_6 octahedron. Early studies have demonstrated that treatment of tetragonal LLZO garnet powders in water or acid leads to the transformation to the cubic polymorph, the direct result of introducing disorder in the Li network through H^+/Li^+ ion exchange [107]. The chemical instability of tetragonal LLZO has been explored extensively in numerous research articles, and thus with a particular focus being placed on LLZO-based garnet SSEs in the cubic phase in this review. Chi *et al*. have demonstrated that cubic LLZO in common with other Li5 and Li6 series garnets experience a rapid and spontaneous Li^+/H^+ exchange reaction upon exposure to water [108]. This proton exchange process is unaccompanied by any structural transformation even with the high exchange rate of 63.6%. The reversible Li^+/H^+ exchange occurs in protonated garnet after being immersed in 2 mol/L LiOH with Li^+ re-entering the lattice while remaining structurally unchanged. Aguadero *et al*. analyzed the proton exchange region in Ga-incorporated LLZO-based garnets based on focused ion beam secondary ion mass spectrometry (FIB-SMS), and revealed the effect of proton-lithium exchange-induced chemical degradation on Li-ion dynamics across the bulk and grain boundaries in highly lithium-conducting garnet electrolytes [109]. There is evidence that prolonged immersion in liquid H_2O at 100 °C re-

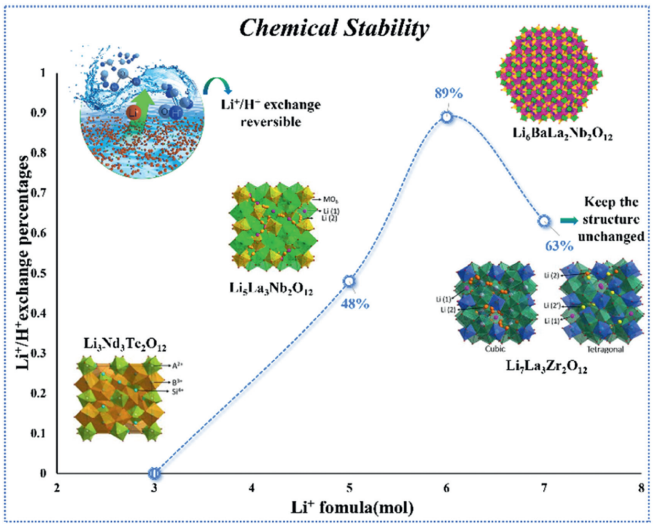

Fig. 6. Schematic diagram of the chemical stability for cubic garnet-based ion conductors as a function of lithium-ion concentration. Reproduced with permission [111]. Copyright 2021, Elsevier; Reproduced with permission [36]. Copyright 2020, American Chemical Society; Reproduced with permission [108]. Copyright 2015, Wiley.

sults in an increase in the thickness of the H-Ga0.15-LLZO region formed *via* H^+/Li^+ exchange, extending as far as 1.35 μm into Ga0.15-LLZO garnet pellets after 30 min. Proton-lithium exchange reactions in lithium-conducting garnet have a detrimental effect on charge carrier transport in bulk and lithium-ion mobility at the solid-state electrolyte/electrode interface. In light of the development of advanced characterization techniques, the occurrence of LiOH on the surface of cubic $Li_{6.4}La_3Zr_{1.4}Ta_{0.6}O_{12}$ garnet under rarefied air has recently been directly observed employing *quasi-in situ* X-ray photoelectron spectroscopy (XPS) [110]. Not only single-atom or double-doped, but high entropy garnet-based oxides that have gained increasing popularity recently are also found to suffer from atmospheric water and carbon dioxide. The Li_2CO_3 impure phase is still evident in the XRD patterns after 60 days of exposure to ambient air despite no obvious decay in ionic conductivity [111,112]. As depicted in Fig. 6, stability in humid atmospheres cannot be generalized to all lithium garnet-type oxides, as the feasibility of Li^+/H^+ exchange is closely related to lithium stoichiometry: the garnet oxide is likely to be sensitive to humidity if the Li^+ concentration is greater than what can be accommodated on the tetrahedral site commonly occupied by Li ions.

3.1.2. Li-site occupation behavior

It is well known that the sensitivity of Li-stuffed LLZO-based garnet oxides to water originates from facile proton-for-lithium exchange [113]. However, changes in the stoichiometric ratio of lithium ions will lead to variations in their distribution within the three-dimensional interstitial space, thus further investigation is imperative to identify the preferential site for proton exchange. Chi *et al.* proposed that cubic LLZO preferentially underwent proton exchange by the most anisotropic 96h site Li in aqueous solution based on electron energy loss spectroscopy (EELS) analysis, resulting in the disappearance of the doublet in Li-K near-edge fine structure [106]. The exchange barely further proceeded after Li was depleted located at the off-center octahedral site, leaving both the 48g and 24d sites largely unaffected. This conclusion has also been confirmed by Wen *et al.* who carried out continuous H^+/Li^+ ion exchange on cubic $Li_{6.75}La_3Nb_{0.25}Zr_{1.75}O_{12}$ powder in distilled water, demonstrating that the octahedral positions occupied with Li in the garnet $B_3C_2O_{12}$ structure are more readily available to exchange with proton since they bond lithium ions less tightly than the tetrahedral positions [114]. The reactivity of cubic LLZO-based garnet- $Li_{6.5}La_3Zr_{1.5}Ta_{0.5}O_{12}$ in water confirms anew the nature underlying the chemical instability for Li-rich materials of this type [115]. NPD combined with NMR techniques reveals that exchanged protons in hydrated garnet displace Li from the octahedral position bridging the 24d tetrahedral site, and building weak O–H bonds with the surrounding oxygen resulting in increasing the octahedral configurations distortion. Additional evidence comes from a single-crystal XRD analysis of H proton entry into cubic Al:LLZO garnet ionic conductors performed over a period of 3 years according to Rettenwander *et al.* [116] It is demonstrated that extensive Li^+/H^+ exchanges have only the result of reducing the mobile Li-ions at the 96h position.

On the contrary, Rettenwander *et al.* have found that the aging of both single crystals as well as Czochralski-grown $Li_6La_3ZrTaO_{12}$ in water or acetic acid at room temperature retains $Ia\bar{3}d$ symmetry but induces a Li^+/H^+ exchange preferable at the Li-occupied tetrahedral site, based on XRD and NPD techniques [117]. Inconsistencies in conclusions can be attributed to differences in garnet compositions and substitution contents, thus impacting the Li^+/H^+-exchange rate, Li^+/H^+-exchange capacity, Li^+/H^+-site occupancy behavior, and even lithium oxide garnet structural stability. Developing universal design rules based on a diversity of components to enhance future material properties.

3.1.3. Li-O bonding interactions

Lithium-oxygen bonding is another critical aspect responsible for the chemical instability of cubic lithium-rich garnet-based oxide ion conductors since it directly affects the extraction of lithium ions from the sublattice. Proton replacing lithium ions enter into the structural interstices accompanied by the breaking of strong Li-O bonds and the formation of weak hydrogen O–H···O bonds, as a result leading to lattice expansion [102]. There are two available sites for Li^+/H^+ ion exchange in cubic LLZO-based garnet. It is generally accepted that tetrahedral 24d sites are skeleton sites and Li-ion trapping sites where Li ions are tightly bound with O and less mobile, while the Li ions at the octahedral 96h sites are more loosely bound and are believed to be responsible for fast Li-ion mobility in the 3D channel [104]. Li-O bond engineering is therefore necessary in order to fundamentally improve the chemical stability of lithium-rich garnet structural oxides. However, high Li^+ conductivity most often arises from weak Li-O bonding in oxide ionic conductors, which accounts precisely for decreased stability under moisture attacks. This phenomenon is also common in inorganic solid ion conductors such as perovskites and sulfides [6]. More calculations based on theoretical principles are imperative in the future to screen suitable elements on a large scale and to modulate the electronic states from the perspective of inorganic solid chemistry in order to obtain the next generation of solid ionic conductors with high conductivity and stability.

3.2. LLZO air exposure-related reaction mechanisms

Garnet-based solid electrolytes are highly susceptible to being attacked by Li_2CO_3 as discussed above, and even calcined samples may have already begun to protonate during cooling in the furnace [118]. Different pathways have been proposed to elucidate the reaction between cubic LLZO and air. Garnet-based electrolytes are able to directly react with CO_2 to form Li_2CO_3 in the absence of H_2O according to the previously reported single-step reaction [119–121]. The reaction pathway described in Eq. 1 is thermodynamically favorable according to DFT calculations but is kinetically slow considering the negligible amount of Li_2CO_3 generated upon the pristine specimen after exposure to dry air [120]. Recently Canepa *et al.* utilized first-principles calculations to elucidate that the individual reaction of H_2O and CO_2 with LLZO is ther-

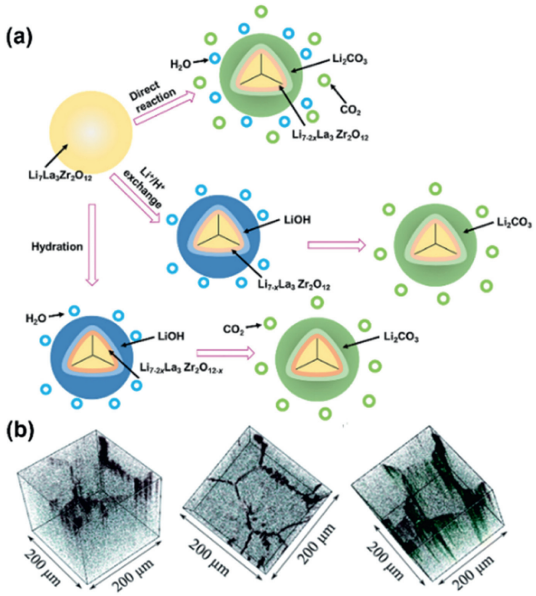

Fig. 7. (a) Multiple possible reaction pathways between garnet-based ceramic particles and humid air. Reproduced with permission [118]. Copyright 2020, American Chemical Society. (b) Three-dimensional reconstruction image depicting the accumulation of OH- corrosion products along grain boundaries near the surface. Reproduced with permission [128]. Copyright 2020, Royal Society of Chemistry.

modynamically more favorable than the co-adsorption of H_2O and CO_2 [122]. But the currently more widely accepted reaction pathway includes two steps [6,99,123]. Water vapor from the environment will be absorbed on the surface of the garnet ceramic pellets upon exposure to humid air, thus initiating the reaction of Li^+/H^+ exchange at specific sites in the structure. A sufficient amount of water is required to be present before or simultaneously with the reaction with CO_2 in order to produce essential intermediate $LiOH{\cdot}H_2O$ following the generation of LiOH. The top layer of Li_2CO_3 is then formed as a result of the carbonating reaction between $LiOH{\cdot}H_2O$ and CO_2 to provide protection for the pellet underneath, as depicted in the following reaction Eqs. 2 and 3 [118,124]. Tang *et al.* validated the above reaction mechanism from the experimental point of view by performing XPS depth profiling on 24 h air-exposed $Li_{6.4}La_3Zr_{1.4}Ta_{0.6}O_{12}$ samples [125]. With increasing sputtering depth, contaminants of $LiOH{\cdot}xH_2O$ and Li_2CO_3 decrease and diminish at about 160 nm, while H-LLZTO increases at the same time and finally turns into LLZTO at about 240 nm as the degree of H^+/Li^+ exchange decreases. The conclusion is generally in agreement with the results of Sakamoto *et al.* performed on raw unmodified LLZO garnet [126]. Fig. 7a visually illustrates the two reaction pathways mentioned above. Although garnet-based ceramic pellets are difficult to escape the fate of contamination once in contact with air, the extent of contaminant formation on their surfaces, the stepwise evolution of contaminants, and the inhomogeneous distributions exhibited are still in need of further investigation with *in situ* characterization and theoretical calculations.

$$Li_7La_3Zr_2O_{12} + x\ CO_2 \rightarrow Li_{7-2x}La_3Zr_2O_{12} + x\ Li_2CO_3 \quad (1)$$

$$Li_7La_3Zr_2O_{12} + x\ H_2O \rightarrow Li_{7-x}H_xLa_3Zr_2O_{12} + x\ LiOH \quad (2)$$

$$LiOH + 1/2\ CO_2 \rightarrow 1/2\ Li_2CO_3 + 1/2\ H_2O \quad (3)$$

Additionally to the grains, amorphous Li_2O and/or Li_2AlO_2 deposited at grain boundaries for garnet-based ceramic solid electrolytes also tend to undergo Li^+/H^+ exchange reactions with H_2O. Jin *et al.* even speculated that corrosion may take place initially at grain boundaries since grain boundaries exhibit a higher interfacial energy making them more susceptible to moisture than grains [127]. The contaminants spread from the grain boundaries and gradually wrap around the whole grain progressively from the outer surface to the inside, so that eventually grain boundary impedances increase significantly as well as grain ionic transport decreases substantially as a result of the formation of LiOH and Li_2CO_3 lithium-ion insulators as well as more new interfaces (Fig. 7b). Grain size in the synthesis and preparation directly affects the number of grain boundaries in garnet ceramic-based solid electrolytes, thereby being tightly related to the chemical stability of the solid electrolyte [128,129]. However, it remains controversial whether ceramic pellets composed of large or small grains are more resistant to humidity-induced erosion, and the optimal size range for the preparation of garnet-based electrolytes with high conductivity and air stability requires further clarification [120,121].

3.3. Structural modifications enhance chemical stability

Solid lithium-rich garnet ceramic pellets exposed to moisture will trigger proton exchange reactions where the spatial orientation of H^+ will severely hinder Li^+ migration in three-dimensional anisotropic channels, thereby lowering the ionic conductance [6]. Moreover, garnet ceramics could even suffer from a phase transition when the degree of ionic exchange is heightened further, resulting in the deterioration of their mechanical properties [130]. Moisture erosion not only has a negative effect on the intrinsic physicochemical properties of ceramic garnet-based oxides, but also batteries assembled based on them weaken the wettability of Li metal on the LLZO substrate due to LiOH and Li_2CO_3 passivation layers formed on the surface thus enlarging the interfacial impedance between the Li anode electrode and the solid-state electrolyte [29,118]. In addition, it is also detrimental to lithium stripping and plating during cycling as the voids formed at the interface during stripping result in an increase in the apparent interfacial resistance, provoking the formation of dendrites from inhomogeneous lithium plating ultimately causing a short circuit [7]. Wise manipulation of atoms to modulate atomic arrangements for building more desirable electrolyte structural frameworks from a solid-state chemistry perspective, ultimately mitigating the adverse effects of ionic exchange and thus fully utilizing the advantages of garnet.

Cui *et al.* incorporated the elements Nb and Y simultaneously into the Zr site of cubic LLZO garnet-based electrolyte, where Y^{3+} with a lower valence was able to compensate for the loss of lithium resulting from the high valence Nb^{5+} introduction and prohibit the substitution of Al^{3+} in the lattice, thus endowing $Li_7La_3ZrNb_{0.5}Y_{0.5}O_{12}$ with excellent chemical stability [131]. The transport properties exhibited by the oxide ionic conductor can be maintained at the order of 10^{-4} S/cm after 1.5 months of exposure to air. Two cubic crystal systems $Li_{6.05}La_3Ga_{0.3}Zr_{1.95}Nb_{0.05}O_{12}$ and $Li_7La_{2.75}Ca_{0.25}Zr_{1.75}Nb_{0.25}O_{12}$ garnets with $Ia\bar{3}d$ space group are designed obtained *via* the similar co-doping strategy, where Ga preferentially occupies the interstitial Li site, Ca primarily replaces the framework La location, and Nb is present only at the Zr position [132]. Due to the difference in doping sites of dopants, the air stability of $Li_{6.05}La_3Ga_{0.3}Zr_{1.95}Nb_{0.05}O_{12}$ garnet was significantly enhanced as a result of modifications implemented in its microstructure. Our team engineered specific functional elements to improve their intrinsic chemical stability *by* identifying the structural features of cubic lithium-rich garnet-based superionic conductors with synergistic control of doping and non-stoichiometry [133]. The optimal composition of $Li_{6.25}Ga_{0.2}La_3Zr_2O_{11.85}F_{0.15}$ (LGLZO-0.15F) garnet demonstrates excellent air durability without noticeable impurity accumulation, even with continuous air exposure for 60 days, owing to the high affinity of the fluorine dopant for lithium occupying the

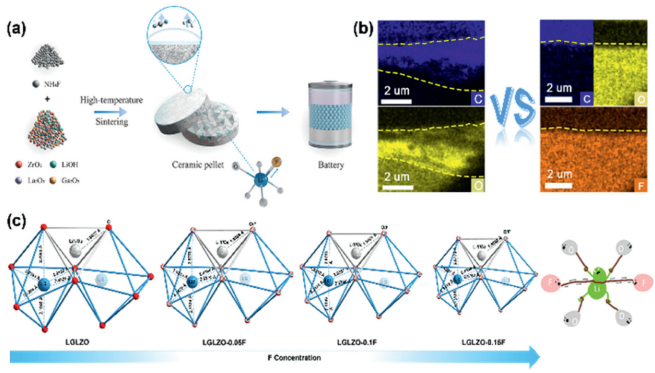

Fig. 8. (a) Schematic diagram of preparing garnet-based ceramic electrolyte with the traditional high-temperature solid-phase method and its assembly into lithium batteries. (b) Comparing the air durability of LGLZO and LGLZO-0.15F pellets after 60 days in ambient air exposure. (c) Mechanism of enhanced chemical stability in cubic Li-stuffed fluorinated garnets. Reproduced with permission [133]. Copyright 2022, American Chemical Society.

octahedral site (Fig. 8). Sholl *et al.* inferred that upon replacing the Zr sites within the LLZO framework structure with Sn or Hf elements based on DFT calculations, $Li_7La_3Sn_2O_{12}$ exhibited higher chemical stability in ambient air than the other two materials, re-emphasizing the crucial role that modulation of intra-structural bonding interactions through elemental compositions plays in the air chemical stability of oxide electrolytes [134].

4. Perspective

The garnet-structured SSEs are considered the most promising candidate for next-generation advanced SSLBs owing to the inherent benefit of high ionic conductivity at room temperature, wide electrochemical window, and excellent stability to Li anodes. Literature search reveals that the number of articles on solid electrolytes has increased year by year within fifteen years (2008–2023), while at the same time the number of reports related to garnet-based ionic conductors has also grown demonstrating its significant influence (Fig. 9). Despite the fact that this type of electrolyte has made significant advances in recent years, commercialization of SSLBs remains on the horizon. Here, we present some perspectives derived from our accumulated knowledge with the hope of promoting its industrialization:

(1) The ionic conductivity of electrolytes is a crucial criterion for researchers to evaluate their performance and determine whether the electrolyte can be further applied in batteries. Multiple generations of exploration have resulted in significant progress in comprehending the conductivity performance of LLZO SSEs. The currently available LLZO SSEs with single-atom doping of Ga, Fe, Ta, and Te were able to obtain high ionic conductivity at room temperature ($>10^{-3}$ S/cm). However, LLZO-based ionic conductors still require considerable development before they reach the heights of ionic conductivity achieved by liquid electrolytes at present. Therefore, researchers also explored how to make improvements to the LLZO sintering process in addition to doping modification. Different sintering mechanisms are able to affect lithium ions volatility in oxide precursors, further responsible for the transformation of the phase structure, and ultimately will have a significant effect on the uniformity, densification, and mechanical performance of the oxide ceramic pellet resulting from sintering. The ionic conductivity of LLZO can be substantially increased by fabricating it into thin films through physical/chemical vapor deposition methods such as radio-frequency sputtering, pulsed laser deposition, and metal-organic chemical vapor deposition. Compared to bulk materials, ultra-thin films are more likely to achieve stable crystal phases as well as reduce grain boundaries and defects, thereby reducing the migration resistance of lithium ions in the material [28]. Since the increasing demand for commercialization and the incoming bottleneck period for increasing ionic conductivity, researchers have turned their attention to stability studies of oxide-based electrolytes especially cubic LLZO-based materials. Stability improvement is expected to greatly reduce storage costs, simplify storage methods, extend the performance retention period, as well as contribute strongly to commercial value. The majority of research studies presently focus on surface engineering from a macro perspective in order to enhance stability. It possesses considerable potential research value for suppressing stability from the origin and reducing the occurrence of stability-reduced reactions viewed from an atomic perspective. Considering stability from an atomic perspective allows for the possibility of suppressing ionic exchange from the beginning and reducing the occurrence of stability-reduced reactions.

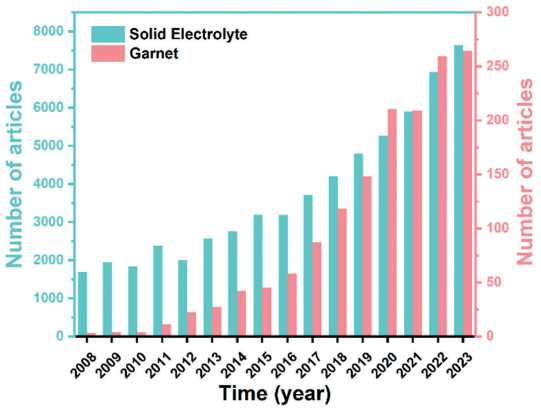

Fig. 9. The literature search reveals the growth in articles on solid electrolytes over the last fifteen years (2008–2023), and garnet-based ionic conductors have also developed rapidly over this period.

(2) High ionic conductivity performance at atmospheric temperature and excellent chemical stability in the ambient environment are considered to be two of the most significant characteristics for oxide-based super-ionic conductors. Ceramic oxide-based electrolytes employed in advanced all-solid-state batteries are expected to possess both properties. However, currently several prevalent oxide ceramic electrolytes such as LATP and LLTO are found to have difficulties simultaneously manifesting them. Research has revealed that the more tightly bound Li atom in LMO gives rise to a higher Li insertion voltage, resulting in higher stability. The theory provides a reasonable explanation for the paradoxical relationship between ionic conductivity and air stability of oxide-type solid electrolytes since strong Li-M bonds are associated with high Li^+ conductivity, which in turn may result in lower stability under wet conditions. Sulfide-based solid electrolytes also suffer from similar difficulties. Therefore, it is imperative to clarify in great detail the inextricable connection between the two properties, relying on Big Data and artificial intelligence (AI) to reasonably build the required atomic arrangement according to the information hidden in the periodic table of elements, thus enabling garnet and even oxide solid electrolytes with excellent ionic conductivity and high chemical stability.

(3) In addition to the exposed issues mentioned above, solid electrolytes also encounter poor contact with the solid anode/cathode, potentially resulting in excessive local current stimulating lithium dendrites growth, eventually resulting in battery short circuits. The interface challenge involves not only the as-assembled contact interface but also the in-progress being developed interface during cycling. A more detailed investigation of the electrolyte-cathode interface is needed. Determining how to address the physical or chemical interface contact in the cathode will assist in better comprehending and optimizing solid-state electrolyte function at a full cell level. Composite electrolytes have the potential to address this difficulty due to their ability to mitigate the disadvantages and promote the advantages of each structural component, thus improving the intrinsic ionic conductivity, mechanical strength, thermal stability, and electrode compatibility of the material. Composite electrolytes provide the ideal solution for constructing solid-state metal lithium batteries with improved solid-solid contacts and reduced interface impedances. By converting the rigid interface into a flexible interface, structural stress can be released during cycling, and volume changes of the electrode during cycling can be suppressed, thus improving the physical and mechanical stability and optimizing the electrochemical performance of the battery. Chemical stability and electrochemical stability refer to the ability of the solid-solid contact interface to maintain the stability of physical and chemical properties at the interface under the action of the external electric field, respectively. Therefore, improving the chemical and electrochemical stability of the solid-solid interface is of great significance for all-solid-state batteries with high energy density. Enhancing the thermal stability problem can significantly bolster the safety performance of the battery and eliminate its potential safety risks thereby ensuring its application is more extensive.

(4) As the core component of all-solid-state batteries, solid-state electrolytes still face numerous challenges in their transition from laboratory to industrial production. Firstly, the synthesis and processing of the material is carried out under strict conditions such as specific temperature and pressure conditions, posing a significant challenge to industrial production. Secondly, ensuring uniformity and reliability of materials during mass production is also a major technical barrier. In addition, solid-state electrolytes encounter considerably more difficulties in assembling batteries and operating interfaces than traditional liquid electrolytes, including contact issues between electrolytes and electrode materials that require innovative technologies and processes to resolve.

Despite these challenges, the prospects for the industrialization of solid-state electrolytes are still favoured by the industry. The continuous development of new materials, advances in production technology, and the realization of economies of scale are gradually reducing the cost of solid-state electrolytes, enabling their use in a variety of applications. Especially in the field of electric vehicles, solid-state batteries are considered a key technology to achieve longer range, faster charging speeds, and better safety. Therefore, in-depth discussions on the industrialization process and challenges faced by solid-state electrolytes will help promote the development and application of this technology, opening up a new chapter in energy and materials science.

5. Conclusion

In summary, the crystal structure defines the dimensionality of interstitial sites as well as their connectivity further directly determining the intrinsic physicochemical properties of crystalline materials including oxide superionic conductors. While the individual properties of the atoms and ions encoded in the periodic table determine basic redox chemistry, embedding it into specific sites within the garnet structure where its peculiar electronic structure and defects will endow this class of materials with fascinating operating potentials, electrochemical capacities, electrochemical stabilization windows, and electronic and ionic conductivities. Structural design and assembly strategies for cubic garnet-based solid electrolytes are necessary to be optimized for all-solid-state batteries. This review will provide a valuable direction for future engineering and optimization of oxide-based ionic conductor materials to achieve higher capacity and energy density.

Declaration of competing interest

The authors declare that they have no known competing financial interests or personal relationships that could have appeared to influence the work reported in this paper.

CRediT authorship contribution statement

Jingyu Shi: Writing – original draft. **Xiaofeng Wu:** Conceptualization. **Yutong Chen:** Investigation. **Yi Zhang:** Investigation, Methodology. **Xiangyan Hou:** Software. **Ruike Lv:** Conceptualization, Visualization. **Junwei Liu:** Software. **Mengpei Jiang:** Methodology, Conceptualization. **Keke Huang:** Conceptualization, Data curation, Formal analysis, Writing – review & editing. **Shouhua Feng:** Conceptualization, Methodology, Validation, Writing – review & editing.

Acknowledgments

This work was supported by the National Natural Science Foundation of China (Nos. 22171102 and 22090044), the National Key R&D Program of China (Nos. 2021YFF0500502 and 2023YFA1506304), the Jilin Province Science and Technology Development Plan (No. 20230101024JC), the "Medicine + X" cross-innovation team of Bethune Medical Department of Jilin University "Leading the Charge with Open Competition" construction project (No. 2022JBGS04), and the Jilin University Graduate Training Office (Nos. 2021JGZ08 and 2022YJSJIP20). The authors thank the beamlines BL13SSW and BL14W1 at the Shanghai Synchrotron Radiation Facility and beamlines MCD-A and MCD-B (Soochow Beamline for Energy Materials) at NSRL.

References

[1] G. Harper, R. Sommerville, E. Kendrick, et al., Nature 575 (2019) 75–86.
[2] Y. Liu, X. Tao, Y. Wang, et al., Science 375 (2022) 739–745.
[3] Y. Zeng, B. Ouyang, J. Liu, et al., Science 378 (2022) 1320–1324.
[4] Y.C. Yin, J.T. Yang, J.D. Luo, et al., Nature 616 (2023) 77–83.
[5] Y. Chen, Z. Wang, X. Li, et al., Nature 578 (2020) 251–255.
[6] R. Chen, Q. Li, X. Yu, et al., Chem. Rev. 120 (2019) 6820–6877.
[7] W. Lu, M. Xue, C. Zhang, Energy Storage Mater. 39 (2021) 108–129.
[8] S. Kalnaus, N.J. Dudney, A.S. Westover, et al., Science 381 (2023) eabg5998.
[9] Y. Li, S. Song, H. Kim, et al., Science 381 (2023) 50–53.
[10] S. Yu, J. Noh, B. Kim, et al., Science 382 (2023) 573–579.
[11] X. Shen, H. Liu, X.-B. Cheng, et al., Energy Storage Mater. 12 (2018) 161–175.
[12] A. Manthiram, X. Yu, S. Wang, Nat. Rev. Mater. 2 (2017) 1–16.
[13] Z. Wu, Z. Xie, A. Yoshida, et al., Renew. Sust. Energ. Rev. 109 (2019) 367–385.
[14] A.K. Mishra, H.A. Chaliyawala, R. Patel, et al., J. Electrochem. Soc. 168 (2021) 080536.
[15] L.Z. Fan, H. He, C.W. Nan, Nat. Rev. Mater. 6 (2021) 1003–1019.
[16] J.F. Ding, R. Xu, C. Yan, et al., Chin. Chem. Lett. 31 (2020) 2339–2342.
[17] F. He, Z. Hu, W. Tang, et al., Adv. Funct. Mater. 32 (2022) 2201465.
[18] Q. Zhao, S. Stalin, C.-Z. Zhao, et al., Nat. Rev. Mater. 5 (2020) 229–252.
[19] X. Zhu, K. Wang, Y. Xu, et al., Energy Storage Mater. 36 (2021) 291–308.
[20] L. Xu, J. Li, H. Shuai, et al., J. Energy Chem. 67 (2022) 524–548.
[21] Z. Gao, H. Sun, L. Fu, et al., Adv. Mater. 30 (2018) 1705702.
[22] J.C. Bachman, S. Muy, A. Grimaud, et al., Chem. Rev. 116 (2016) 140–162.
[23] X. Ke, Y. Wang, G. Ren, et al., Energy Storage Mater. 26 (2020) 313–324.

[24] C. Wang, J.T. Kim, C. Wang, et al., Adv. Mater. 35 (2023) 2209074.
[25] C. Li, Y. Qiu, Y. Zhao, et al., Chin. Chem. Lett. 35 (2024) 108846.
[26] Y. Wu, S. Wang, H. Li, et al., InfoMat 3 (2021) 827–853.
[27] T. Famprikis, P. Canepa, J.A. Dawson, et al., Nat. Mater. 18 (2019) 1278–1291.
[28] S. Ramakumar, C. Deviannapoorani, L. Dhivya, et al., Prog. Mater. Sci. 88 (2017) 325–411.
[29] A.M. Abakumov, S.S. Fedotov, E.V. Antipov, et al., Nat. Commun. 11 (2020) 4976.
[30] C. Wang, J. Liang, J.T. Kim, et al., Sci. Adv. 8 (2022) eadc9516.
[31] Y. Chen, K. Wen, T. Chen, et al., Energy Storage Mater. 31 (2020) 401–433.
[32] R. Chen, W. Qu, X. Guo, et al., Mater. Horizons. 3 (2016) 487–516.
[33] R. Murugan, V. Thangadurai, W. Weppner, Angew. Chem. Int. Ed. 46 (2007) 7778–7781.
[34] S. Hu, Y.F. Li, R. Yang, et al., Ceram. Int. 44 (2018) 6614–6618.
[35] W. Luo, Y. Gong, Y. Zhu, et al., Adv. Mater. 29 (2017) 1606042.
[36] C. Wang, K. Fu, S.P. Kammampata, et al., Chem. Rev. 120 (2020) 4257–4300.
[37] Y.Z. Zhu, X.F. He, Y.F. Mo, J. Mater. Chem. A 4 (2016) 3253–3266.
[38] J. Gao, J.X. Zhu, X.L. Li, et al., Adv. Funct. Mater. 31 (2021) 2001918.
[39] X. He, Y. Zhu, Y. Mo, Nat. Commun. 8 (2017) 15893.
[40] E.J. Cussen, J. Mater. Chem. 20 (2010) 5167–5173.
[41] S. Abouali, C.-H. Yim, A. Merati, et al., ACS. Energy Lett. 6 (2021) 1920–1941.
[42] V. Thangadurai, S. Narayanan, D. Pinzaru, Chem. Soc. Rev. 43 (2014) 4714–4727.
[43] A.J. Samson, K. Hofstetter, S. Bag, et al., Energy Environ. Sci. 12 (2019) 2957–2975.
[44] M.P. O'Callaghan, D.R. Lynham, E.J. Cussen, et al., Chem. Mater. 18 (2006) 4681–4689.
[45] M.P. O'Callaghan, A.S. Powell, J.J. Titman, et al., Chem. Mater. 20 (2008) 2360–2369.
[46] H. Peng, Q. Wu, L. Xiao, J. Sol-Gel Sci. Technol. 66 (2013) 175–179.
[47] E.J. Cussen, Chem. Commun. (2006) 412–413.
[48] V. Thangadurai, H. Kaack, W.J. Weppner, J. Am. Ceram. Soc. 86 (2003) 437–440.
[49] V. Thangadurai, W. Weppner, J. Solid State Chem. 179 (2006) 974–984.
[50] V. Thangadurai, W. Weppner, J. Am. Ceram. Soc. 88 (2005) 411–418.
[51] M.P. O'Callaghan, E.J. Cussen, Chem. Commun. (2007) 2048–2050.
[52] V. Thangadurai, W. Weppner, Adv. Funct. Mater. 15 (2005) 107–112.
[53] J. Awaka, N. Kijima, Y. Takahashi, et al., Solid State Ionics 180 (2009) 602–606.
[54] J. Percival, E. Kendrick, P. Slater, Mater. Res. Bull. 43 (2008) 765–770.
[55] H. Xie, Y. Li, J. Han, et al., J. Electrochem. Soc. 159 (2012) A1148.
[56] R. Murugan, W. Weppner, P. Schmid-Beurmann, et al., Mater. Res. Bull. 43 (2008) 2579–2591.
[57] J. Awaka, A. Takashima, K. Kataoka, et al., Chem. Lett. 40 (2011) 60–62.
[58] J. Awaka, N. Kijima, H. Hayakawa, et al., J. Solid State Chem. 182 (2009) 2046–2052.
[59] D. Rettenwander, A. Welzl, L. Cheng, et al., Inorg. Chem. 54 (2015) 10440–10449.
[60] F. Sun, Y. Yang, S. Zhao, et al., ACS. Energy Lett. 7 (2022) 2835–2844.
[61] P. Bottke, D. Rettenwander, W. Schmidt, et al., Chem. Mater. 27 (2015) 6571–6582.
[62] T. Thompson, J. Wolfenstine, J.L. Allen, et al., J. Mater. Chem. A 2 (2014) 13431–13436.
[63] Z. Qin, Y. Xie, X. Meng, et al., J. Eur. Ceram. Soc. 43 (2023) 2023–2032.
[64] H. Yang, N. Wu, Energy Sci. Eng. 10 (2022) 1643–1671.
[65] J.F. Wu, E.Y. Chen, Y. Yu, et al., ACS Appl. Mater. Interfaces 9 (2017) 1542–1552.
[66] E. Rangasamy, J. Wolfenstine, J. Sakamoto, Solid State Ionics 206 (2012) 28–32.
[67] E. Rangasamy, J. Wolfenstine, J. Allen, et al., J. Power Sources 230 (2013) 261–266.
[68] B. Dong, S.R. Yeandel, P. Goddard, et al., Chem. Mater. 32 (2019) 215–223.
[69] R. Wagner, D. Rettenwander, G.J. Redhammer, et al., Inorg. Chem. 55 (2016) 12211–12219.
[70] Y. Li, J.T. Han, C.A. Wang, et al., J. Mater. Chem. 22 (2012) 15357–15361.
[71] W.G. Zeier, Dalton. Trans. 43 (2014) 16133–16138.
[72] R. Inada, K. Kusakabe, T. Tanaka, et al., Solid State Ionics 262 (2014) 568–572.
[73] S. Ramakumar, L. Satyanarayana, S.V. Manorama, et al., Phys. Chem. Chem. Phys. 15 (2013) 11327–11338.
[74] K.C. Santosh, R.C. Longo, K. Xiong, et al., Solid State Ionics 261 (2014) 100–105.
[75] L. Buannic, B. Orayech, J.M. Lopez Del Amo, et al., Chem. Mater. 29 (2017) 1769–1778.
[76] M. Liu, B. Li, S. Zhang, et al., ACS Appl. Energy Mater. 5 (2022) 7559–7570.
[77] D. Rettenwander, G.n. Redhammer, F. Preishuber-Pflügl, et al., Chem. Mater. 28 (2016) 2384–2392.
[78] Y.X. Xiang, G. Zheng, G. Zhong, et al., Solid State Ionics 318 (2018) 19–26.
[79] D. Wang, G. Zhong, W.K. Pang, et al., Chem. Mater. 27 (2015) 6650–6659.
[80] C. Bernuy-Lopez, W. Manalastas Jr, J.M. Lopez del Amo, et al., Chem. Mater. 26 (2014) 3610–3617.
[81] J. Zhao, X. Wang, T. Wei, et al., J. Energy Storage 68 (2023) 107693.
[82] H. Xie, J.A. Alonso, Y. Li, et al., Chem. Mater. 23 (2011) 3587–3589.
[83] T. Thompson, A. Sharafi, M.D. Johannes, et al., Adv. Energy Mater. 5 (2015) 1500096.
[84] H. Nozaki, M. Harada, S. Ohta, et al., Solid State Ionics 262 (2014) 585–588.
[85] M.M. Ahmad, RSC Adv. 5 (2015) 25824–25829.
[86] V. Gajraj, A. Kumar, S. Indris, et al., Ceram. Int. 48 (2022) 29238–29246.
[87] B. Zhang, R. Tan, L. Yang, et al., Energy Storage Mater. 10 (2018) 139–159.
[88] X. Zhang, C. Li, W. Liu, et al., Solid State Ionics 369 (2021) 115713.
[89] N.V. Kireeva, A.Y. Tsivadze, V.S. Pervov, Solid State Ionics 399 (2023) 116293.
[90] X. Xiang, F. Chen, W. Yang, et al., J. Am. Ceram. Soc. 103 (2019) 2483–2490.
[91] Y. Chen, T. Wang, H. Chen, et al., Matter. 6 (2023) 1530–1541.
[92] F. Chen, L. Xu, J. Li, et al., Ionics 26 (2020) 3193–3198.
[93] A.G. Squires, D.O. Scanlon, B.J. Morgan, Chem. Mater. 32 (2019) 1876–1886.
[94] M. Kubicek, A. Wachter-Welzl, D. Rettenwander, et al., Chem. Mater. 29 (2017) 7189–7196.
[95] Z. Ma, B. Zhao, W. Li, et al., Ionics 28 (2022) 2673–2683.
[96] Y. Zhu, M. Chon, C.V. Thompson, et al., Angew. Chem. Int. Ed. 62 (2023) e2023045.
[97] T. Kawaguchi, K. Sugihara, N. Sakamoto, et al., J. Ceram. Soc. Jpn. 128 (2020) 700–705.
[98] C. Chen, K.X. Wang, H.Y. He, et al., Small 19 (2023) 2205550.
[99] K. Hofstetter, A.J. Samson, S. Narayanan, et al., J. Power Sources 390 (2018) 297–312.
[100] L. Cheng, W. Chen, M. Kunz, et al., ACS Appl. Mater. Interfaces 7 (2015) 2073–2081.
[101] Y.T. Li, X. Chen, A. Dolocan, et al., J. Am. Chem. Soc. 140 (2018) 6448–6455.
[102] C. Galven, J. Dittmer, E. Suard, et al., Chem. Mater. 24 (2012) 3335–3345.
[103] F. Gam, C. Galven, A. Bulou, et al., Inorg. Chem. 53 (2014) 931–934.
[104] L. Truong, V. Thangadurai, Chem. Mater. 23 (2011) 3970–3977.
[105] S. Narayanan, F. Ramezanipour, V. Thangadurai, Inorg. Chem. 54 (2015) 6968–6977.
[106] C. Galven, G. Corbel, F.Le Berre, et al., Inorg. Chem. 55 (2016) 12872–12880.
[107] G. Larraz, A. Orera, J. Sanz, et al., J. Mater. Chem. A 3 (2015) 5683–5691.
[108] C. Ma, E. Rangasamy, C.D. Liang, et al., Angew. Chem. Int. Ed. 54 (2015) 129–133.
[109] R.H. Brugge, A.K.O. Hekselman, A. Cavallaro, et al., Chem. Mater. 30 (2018) 3704–3713.
[110] Y.F. Zhou, A.S. Gao, M.Q. Duan, et al., ACS Appl. Mater. Interfaces 15 (2023) 45465–45474.
[111] S. Huang, M.M. Shang, K.L. Peng, et al., J. Lumines. 243 (2022) 118649.
[112] C.H. Kuo, A.Y. Wang, H.Y. Liu, et al., APL Mater. 10 (2022) 121104.
[113] R.J. Ye, M. Ihrig, N. Imanishi, et al., ChemSusChem 14 (2021) 4397–4407.
[114] C. Liu, K. Rui, C. Shen, et al., J. Power Sources 282 (2015) 286–293.
[115] Y.T. Li, J.T. Han, S.C. Vogel, et al., Solid State Ionics 269 (2015) 57–61.
[116] C. Hiebl, D. Young, R. Wagner, et al., J. Phys. Chem. C 123 (2019) 1094–1098.
[117] G.J. Redhammer, P. Badami, M. Meven, et al., ACS Appl. Mater. Interfaces 13 (2021) 350–359.
[118] H.Y. Huo, J. Luo, V. Thangadurai, et al., ACS Energy Lett. 5 (2020) 252–262.
[119] Y.X. Wang, W. Lai, J. Power Sources 275 (2015) 612–620.
[120] L. Cheng, C.H. Wu, A. Jarry, et al., ACS Appl. Mater. Interfaces 7 (2015) 17649–17655.
[121] W.H. Xia, B.Y. Xu, H.N. Duan, et al., ACS Appl. Mater. Interfaces 8 (2016) 5335–5342.
[122] Y.H. Li, A.M. Prabhu, T.S. Choksi, et al., J. Mater. Chem. A 10 (2022) 4960–4973.
[123] Y. Arinicheva, X. Guo, M.T. Gerhards, et al., Chem. Mater. 34 (2022) 1473–1480.
[124] W.H. Xia, B.Y. Xu, H.A. Duan, et al., J. Am. Ceram. Soc. 100 (2017) 2832–2839.
[125] J. Leng, H.Y. Wang, H.M. Liang, et al., ACS Appl. Energy Mater. 5 (2022) 5108–5116.
[126] A. Sharafi, S.H. Yu, M. Naguib, et al., J. Mater. Chem. A 5 (2017) 13475–13487.
[127] Y. Jin, P.J. McGinn, J. Power Sources 239 (2013) 326–331.
[128] R.H. Brugge, F.M. Pesci, A. Cavallaro, et al., J. Mater. Chem. A 8 (2020) 14265–14276.
[129] W. Jeong, S.S. Park, J. Yun, et al., Energy Storage Mater. 54 (2023) 543–552.
[130] S. Kobi, A. Mukhopadhyay, J. Eur. Ceram. Soc. 38 (2018) 4707–4718.
[131] J.L. Gai, E.Q. Zhao, F.R. Ma, et al., J. Eur. Ceram. Soc. 38 (2018) 1673–1678.
[132] L.H. Abrha, T.T. Hagos, Y. Nikodimos, et al., ACS Appl. Mater. Interfaces 12 (2020) 25709–25717.
[133] J.Y. Shi, G. Sun, L.P. Li, et al., ACS. Energy Lett. 8 (2022) 48–55.
[134] S.G. Kang, D.S. Sholl, J. Phys. Chem. C 118 (2014) 17402–17406.